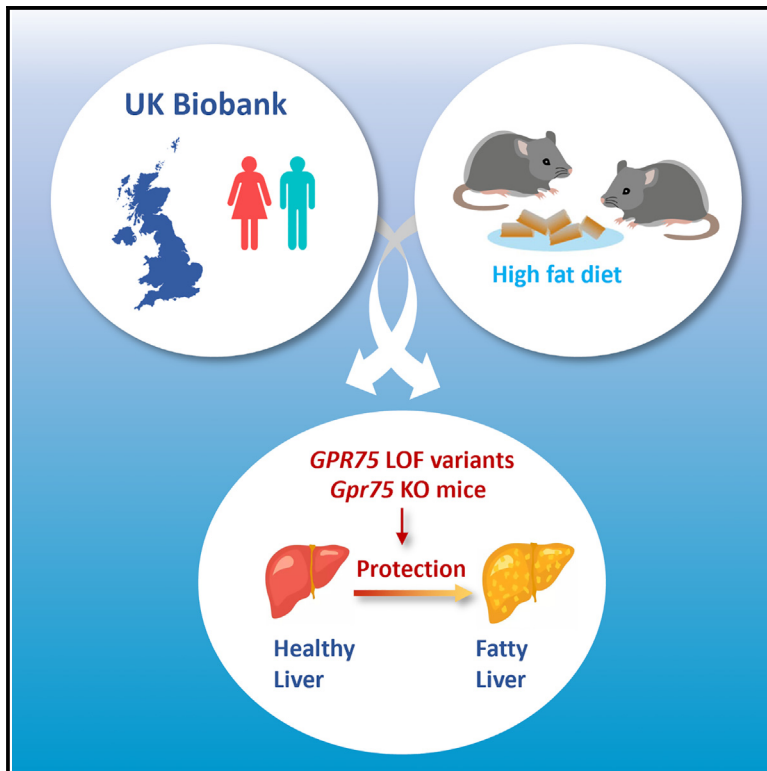


# Cell Metabolism

## Loss of *GPR75* protects against non-alcoholic fatty liver disease and body fat accumulation

### Graphical abstract



### Authors

Alasdair Leeson-Payne, Jean Iyinkkel, Cameron Malcolm, ..., Giles S.H. Yeo, Fiona Murray, Lora K. Heisler

### Correspondence

fmurray@abdn.ac.uk (F.M.),  
lora.heisler@abdn.ac.uk (L.K.H.)

### In brief

Leeson-Payne et al. identify that mutations in orphan receptor GPR75 are protective against the development of non-alcoholic fatty liver disease. These findings provide a much-needed novel treatment target for a prevalent disease in the global population.

### Highlights

- Hypothalamic RNA-seq revealed *Gpr75* co-expression with hunger-promoting neurons
- *Gpr75* knockout mice calibrate intake of palatable, high-fat diet to remain in energy balance
- A sex effect in adiposity features was detected in people and mice with *GPR75* mutations
- Mutations in *GPR75* in people and mice protect against fatty liver disease



Article

# Loss of *GPR75* protects against non-alcoholic fatty liver disease and body fat accumulation

Alasdair Leeson-Payne,<sup>1,7</sup> Jean Iyinkkel,<sup>2,7</sup> Cameron Malcolm,<sup>2</sup> Brian Y.H. Lam,<sup>4</sup> Nadine Sommer,<sup>1</sup> Georgina K.C. Dowsett,<sup>4</sup> Pablo B. Martinez de Morentin,<sup>1</sup> Dawn Thompson,<sup>2</sup> Alasdair Mackenzie,<sup>2</sup> Raffaella Chianese,<sup>1</sup> Katherine Kentistou,<sup>5</sup> Eugene J. Gardner,<sup>5</sup> John R.B. Perry,<sup>4,5</sup> Felix Grassmann,<sup>6</sup> John R. Speakman,<sup>3</sup> Justin J. Rochford,<sup>1</sup> Giles S.H. Yeo,<sup>4</sup> Fiona Murray,<sup>2,\*</sup> and Lora K. Heisler<sup>1,8,\*</sup>

<sup>1</sup>The Rowett Institute, University of Aberdeen, Aberdeen, UK

<sup>2</sup>Institute of Medical Sciences, University of Aberdeen, Aberdeen, UK

<sup>3</sup>School of Biological Sciences, University of Aberdeen, Aberdeen, UK

<sup>4</sup>Wellcome-MRC Institute of Metabolic Science-Metabolic Research Laboratories, Medical Research Council Metabolic Diseases Unit, University of Cambridge, Cambridge, UK

<sup>5</sup>Medical Research Council Epidemiology Unit, Wellcome-MRC Institute of Metabolic Science, University of Cambridge, Cambridge, UK

<sup>6</sup>Institute for Clinical Research and Systems Medicine, Health and Medical University, Potsdam, Germany

<sup>7</sup>These authors contributed equally

<sup>8</sup>Lead contact

\*Correspondence: [fmurray@abdn.ac.uk](mailto:fmurray@abdn.ac.uk) (F.M.), [lora.heisler@abdn.ac.uk](mailto:lora.heisler@abdn.ac.uk) (L.K.H.)

<https://doi.org/10.1016/j.cmet.2024.03.016>

## SUMMARY

Approximately 1 in 4 people worldwide have non-alcoholic fatty liver disease (NAFLD); however, there are currently no medications to treat this condition. This study investigated the role of adiposity-associated orphan G protein-coupled receptor 75 (GPR75) in liver lipid accumulation. We profiled *Gpr75* expression and report that it is most abundant in the brain. Next, we generated the first single-cell-level analysis of *Gpr75* and identified a subpopulation co-expressed with key appetite-regulating hypothalamic neurons. CRISPR-Cas9-deleted *Gpr75* mice fed a palatable western diet high in fat adjusted caloric intake to remain in energy balance, thereby preventing NAFLD. Consistent with mouse results, analysis of whole-exome sequencing data from 428,719 individuals (UK Biobank) revealed that variants in *GPR75* are associated with a reduced likelihood of hepatic steatosis. Here, we provide a significant advance in understanding of the expression and function of GPR75, demonstrating that it is a promising pharmaceutical target for NAFLD treatment.

## INTRODUCTION

Non-alcoholic fatty liver disease (NAFLD) has emerged as a leading cause of chronic liver disease; however, there are currently no approved medications to specifically treat this condition. NAFLD is characterized by the accumulation of excess fat in the liver, and as the disease advances, it promotes fibrosis, steatosis, and non-alcoholic steatohepatitis (NASH).<sup>1</sup> Prolonged NASH can damage the liver, progressing to cirrhosis, hepatocellular carcinoma, and/or liver failure.<sup>1</sup> Overweight and obesity are frequently comorbid with NAFLD, with approximately 75% of overweight individuals and 90% of individuals with extreme obesity affected by NAFLD.<sup>2,3</sup> Obesity also significantly increases death rates in patients suffering from NAFLD.<sup>3</sup> NAFLD in obesity is believed to result from unhealthy, dysfunctional adipose tissue and/or an inability to further expand adipose tissue to safely store lipids. This leads to overflow of lipids and their accumulation in the liver. NAFLD is also observed in conditions in which adipose expansion is constrained, such as in syndromes of lipodystrophy, conditions typically associated with

low to normal body mass indexes (BMIs). Therefore, the relationship between NAFLD and BMI is not simple.<sup>4</sup> The current treatment strategy for NAFLD is behavioral modification, increasing physical activity and decreasing food intake to promote weight loss.<sup>5</sup> However, approximately 80% of people losing weight through lifestyle modification regain weight, illustrating the need for additional treatment options.<sup>6</sup>

Very little is known about orphan G protein-coupled receptor 75 (GPR75), a receptor that has garnered intense interest following a recent report from a large-scale human exome study revealing *GPR75* variants are associated with lower body fat and BMI.<sup>7</sup> Likewise, targeted genetic inactivation of *Gpr75* in mice prevents dietary-induced obesity (DIO),<sup>7–9</sup> suggesting that this receptor plays a fundamental role in body weight regulation. However, the mechanisms via which loss of *GPR75* fosters lower body fat and BMI have not been defined. Given that most genes whose disruption promotes leanness in people have been revealed to cause a form of lipodystrophy, which is associated with increased risk of fatty liver, it is important to establish the effects of *GPR75* perturbation on hepatic lipid accumulation. Here,



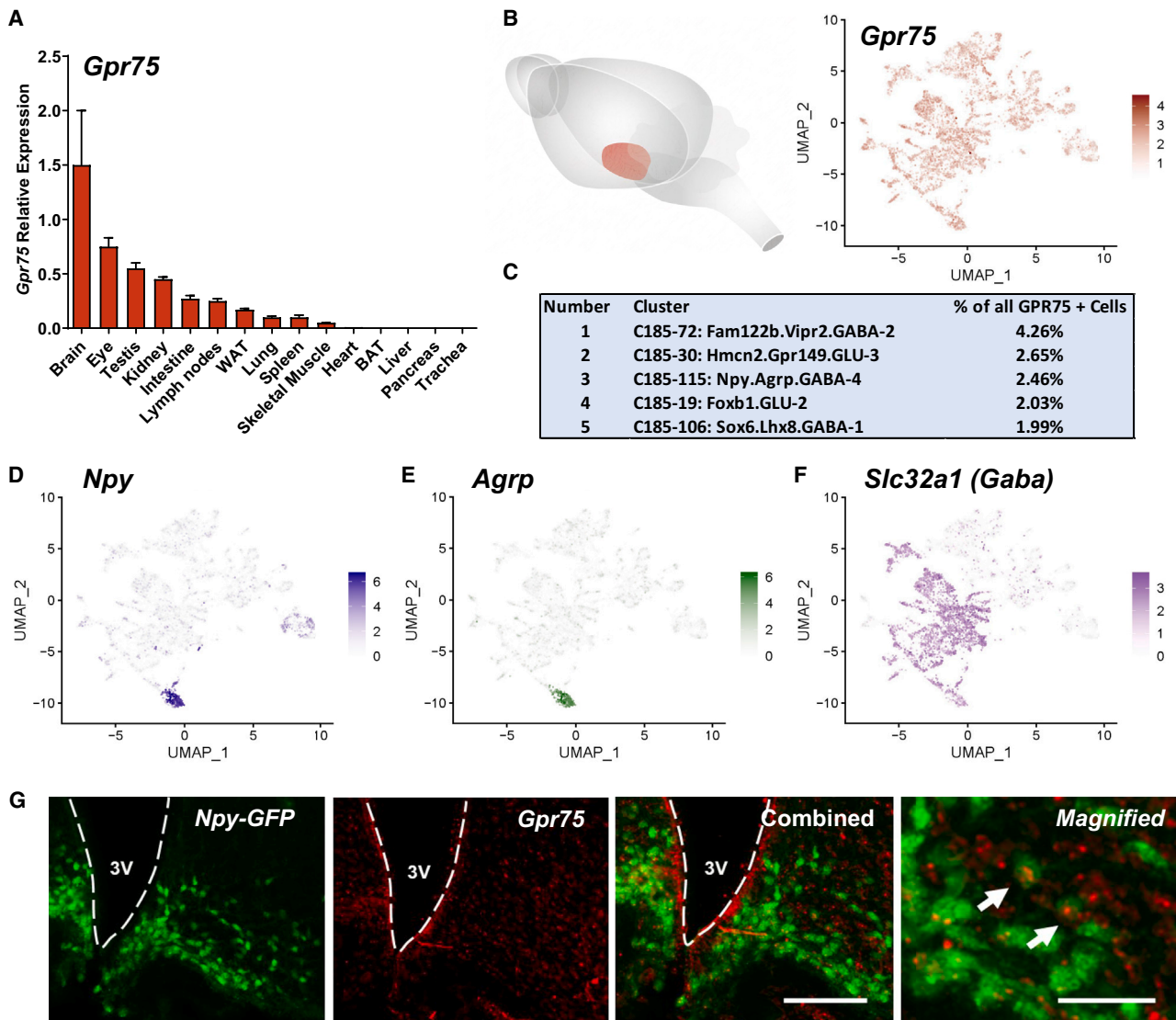


**Figure 1. Characterization of *Gpr75* expression**

(A) Expression of *Gpr75* mRNA across mouse tissues measured by real-time qPCR. (B) Depiction of widespread expression of *Gpr75* within mouse hypothalamus (red). UMAP plot of *Gpr75* expression across hypothalamic nuclei population from HypoMap dataset. (C) Co-expression analysis identified top neuronal clusters in *Gpr75*-positive nuclei. (D–F) Feature plots showing co-expression in *Gpr75*-positive population with (D) neuropeptide Y (*Npy*), (E) agouti-related peptide (*AgRP*), and (F) GABA vesicle uptake protein solute carrier family 32 member 1 (*Slc32a1*). (G) Histological validation of co-expression with *Npy*/AgRP/GABA (NAG) neurons in the arcuate nucleus of the hypothalamus. Expression of *Npy* (green using *Npy-GFP* mice) and detection of *Gpr75* by RNAScope (red). Combined overlay of images confirms co-expression in a subset of NAG neurons. Scale bar, 100  $\mu$ m; magnified scale bar, 50  $\mu$ m.

we specifically examined the function of GPR75 in lipid accumulation relevant to NAFLD.

## RESULTS

### Single-cell RNA-seq and histochemical characterization of hypothalamic *Gpr75* cells

We first profiled *Gpr75* mRNA expression in mice and report that it is most abundantly expressed in the brain and has negligible expression in liver (Figure 1A). Given its abundance in the brain,

we began by mapping *Gpr75* mRNA expression using *in situ* hybridization (RNAScope). We found that it is widely distributed throughout the brain, including (but not restricted to) regions associated with energy homeostasis such as the hypothalamus (Figure S1).

We next performed a detailed characterization of its expression within the hypothalamus, a principal region regulating adiposity, to examine possible mechanisms through which *Gpr75* modulates lipid accumulation. We interrogated HypoMap, a large integrated single-cell RNA sequencing (RNA-seq) dataset consisting of 18



single-cell RNA-seq datasets of the mouse hypothalamus.<sup>10</sup> Out of 384,925 cells in HypoMap, 11,970 cells were *Gpr75* positive (unique molecular identifier [UMI] count  $\geq 1$ ), reflecting 3.12% of all cells. The majority of *Gpr75*-positive cells were neurons (10,609 cells, 88.6%). We next focused on *Gpr75*<sup>+VE</sup> neurons and regenerated the uniform manifold approximation and projection (UMAP) plot (Figure 1B). There are seven levels of clustering in HypoMap, allowing for the display of increasing levels of granularity within the dataset. At cluster level C185, *Gpr75*<sup>+VE</sup> cells are present in all 130 neuronal clusters (Table S1A). The largest cluster of *Gpr75*-expressing cells is C185-72: Fam122b.Vipr2.GABA-2 (4.26% of all *Gpr75*<sup>+VE</sup> cells), which are predicted to be located in suprachiasmatic nucleus (SCN) (Figure 1C). The other 4 top clusters of *Gpr75*<sup>+VE</sup> cells are C185-30: Hmcn2.Gpr149.GLU-3 (2.65%), C185-115: Npy.Agrp.GABA-4 (2.46%), C185-19: Foxb1-GLU-2 (2.03%), and C185-106: Sox6.Lhx8.GABA-1 (1.99%) (Figures 1C–1F).

We further characterized neuropeptide Y (Npy), agouti-related peptide (Agrp), and GABA (“NAG”) co-expressing neurons because they are key regulators of appetite and adiposity.<sup>11</sup> Specifically, activation of NAG neurons potently stimulates feeding, whereas NAG neuron ablation in adult mice reduces food intake, resulting in weight loss.<sup>12–15</sup> We adopted a histological approach to confirm *Gpr75* co-expression with NAG neurons using *Npy-hrGFP* mice. We previously reported that 99.5% of *Npy-GFP* neurons express *Agrp* mRNA.<sup>16</sup> Consistent with our findings from HypoMap, we observed widespread hypothalamic expression of *Gpr75* and that a small subset of *Gpr75* (using RNAScope) is co-expressed with NAG neurons (using *Npy-hrGFP* mice). Focusing specifically on NAG cells, we found approximately a quarter of NAG neurons co-expressed *Gpr75* (Figure 1G). *Agrp* competes for action with pro-opiomelanocortin (Pomc)-derived peptides at the melanocortin 4 receptor (MC4R) to regulate body weight.<sup>11</sup> Capitalizing on this neurobiological effect and demonstrating translational relevance, the MC4R agonist setmelanotide is used to treat genetic forms of extreme obesity.<sup>17</sup> Our data indicate that *Gpr75* is a new player influencing the activity of approximately a quarter of NAG neurons. We conclude that *Gpr75* is heterogeneously expressed in the brain, including regions and specific neuronal populations significantly modulating food intake and lipid accumulation.

### *Gpr75* KO mice adjust HFD intake to be equivalent to chow caloric intake

We examined whether *Gpr75* is required for normal appetite control by generating a mouse line without functional *Gpr75*. A CRISPR-Cas9 approach was used to create a 5 base pair (bp) deletion in *Gpr75*, introducing a premature stop in the *Gpr75* sequence (*Gpr75* knockout [KO]; Figures 2A and 2B). We report that male and female *Gpr75* KO mice consumed a similar number of calories to wild-type (WT) mice when fed a chow diet (Figures 2D–2G). However, when provided with a palatable, high-calorie diet high in fat (42% fat; high-fat diet [HFD]), male and female *Gpr75* KO mice adjusted intake to maintain calories equivalent to chow consumption (Figures 2D–2G). This occurred despite a clear preference for HFD as compared with chow when given a choice between the two diets, which illustrates that the lowered HFD intake is not due to palatability (Figures S2N and S2O). By contrast, WT mice significantly increased daily caloric intake on an HFD (Figures 2D–2G), promoting obesity (Figure 3). We performed meal pattern analysis to examine ingestive behavior in mice provided with the two different diets. Meal structure analysis revealed that mice reduced daily meal size (measured in grams) and duration when presented with the HFD compared with chow, consistent with the HFD being more calorific and satiating than chow (Figures 2H and 2I). WT mice increased their daily caloric intake on the HFD (Figures 2D–2G) by having more frequent meals (Figure 2J) with a smaller interval between meals (Figure 2K) compared with the chow diet. The meal structure analysis showed that *Gpr75* KO mice adjusted meal size and duration but did not change meal frequency or time between meals when provided with the HFD compared with chow (Figures 2H–2L). These results indicate that *Gpr75* KO mice consume an appropriate number of calories to maintain energy balance when provided with a palatable, high-calorie diet.

We also assessed energy expenditure and observed that *Gpr75* KO mice were significantly more physically active (Figures 2M–2P and S2A–S2D), particularly during the onset of the dark phase (Figures S2H and S2K). However, no overall differences between genotypes in daily expenditure were detected when mice were fed chow or after acute (4 days) HFD exposure (Figures 2Q and 2R). Energy expenditure was also quantified in mice maintained on HFD for 4.5 months. Minimum metabolic

(C) Schematic of study design in TSE PhenoMaster cages and assessment parameters.

(D and E) (D) Daily caloric food intake over 4 days of chow diet and 4 days of high-fat diet (HFD) (ANOVA time  $\times$  genotype  $F_{(7, 84)} = 2.794, p = 0.01, n = 7$  per group) and (E) average daily food intake by caloric value over 7 days of chow diet and 7 days of HFD (ANOVA diet  $\times$  genotype  $F_{(1, 24)} = 12.71, p = 0.001; n = 7$  per group) in male *Gpr75* KO and WT littermates.

(F and G) (F) Daily food intake by caloric value over 4 days of chow diet and 4 days of HFD (ANOVA time  $\times$  genotype  $F_{(7, 88)} = 4.080, p = 0.0001, n = 6$  per group) and (G) average daily food intake by caloric value over 7 days of chow diet and 7 days of HFD in female *Gpr75* KO and WT littermate mice (ANOVA time  $\times$  genotype  $F_{(1, 26)} = 4.919, p = 0.03; n = 6$  per group).

(H–L) Meal pattern analysis of male and female *Gpr75* KO and WT littermate mice calculated as daily average. *Gpr75* KO and WT mice exhibit decreased (H) meal size (ANOVA diet  $F_{(1, 27)} = 54.71, p < 0.0001; n = 17$  [WT] and  $n = 12$  [KO]) and (I) meal duration on HFD compared with chow diet (ANOVA genotype  $F_{(1, 27)} = 24.56, p < 0.0001; n = 17$  [WT] and  $n = 12$  [KO]). WT mice (but not *Gpr75* KO mice) provided with an HFD increase (J) meal frequency (ANOVA diet  $F_{(1, 27)} = 6.109, p = 0.02; n = 17$  [WT] and  $n = 12$  [KO]) and reduced (K) intermeal interval (ANOVA time  $\times$  genotype  $F_{(1, 27)} = 4.329, p = 0.047; n = 17$  [WT] and  $n = 12$  [KO]). (L) *Gpr75* KO and WT mice exhibit the same eating rate on both diets (ANOVA diet  $F_{(1, 27)} = 1.294, p = 0.25; n = 17$  [WT] and  $n = 12$  [KO]).

(M and O) (M) Male and (O) female *Gpr75* KO mice have higher average spontaneous daily activity on both chow (red) and HFD (blue) compared with WT mice fed chow (white) and HFD (gray).

(N and P) Representative heatmaps illustrating 24 h cage activity pattern measured by total individual beambreaks in (N) male and (P) female HFD-fed *Gpr75* KO and WT littermate mice (scale: low activity white, high activity red).

(Q and R) *Gpr75* KO and WT (Q) male and (R) female littermates have similar daily energy expenditure. \* $p < 0.05$ , \*\* $p < 0.01$ , \*\*\* $p < 0.001$ , \*\*\*\* $p < 0.0001$ .

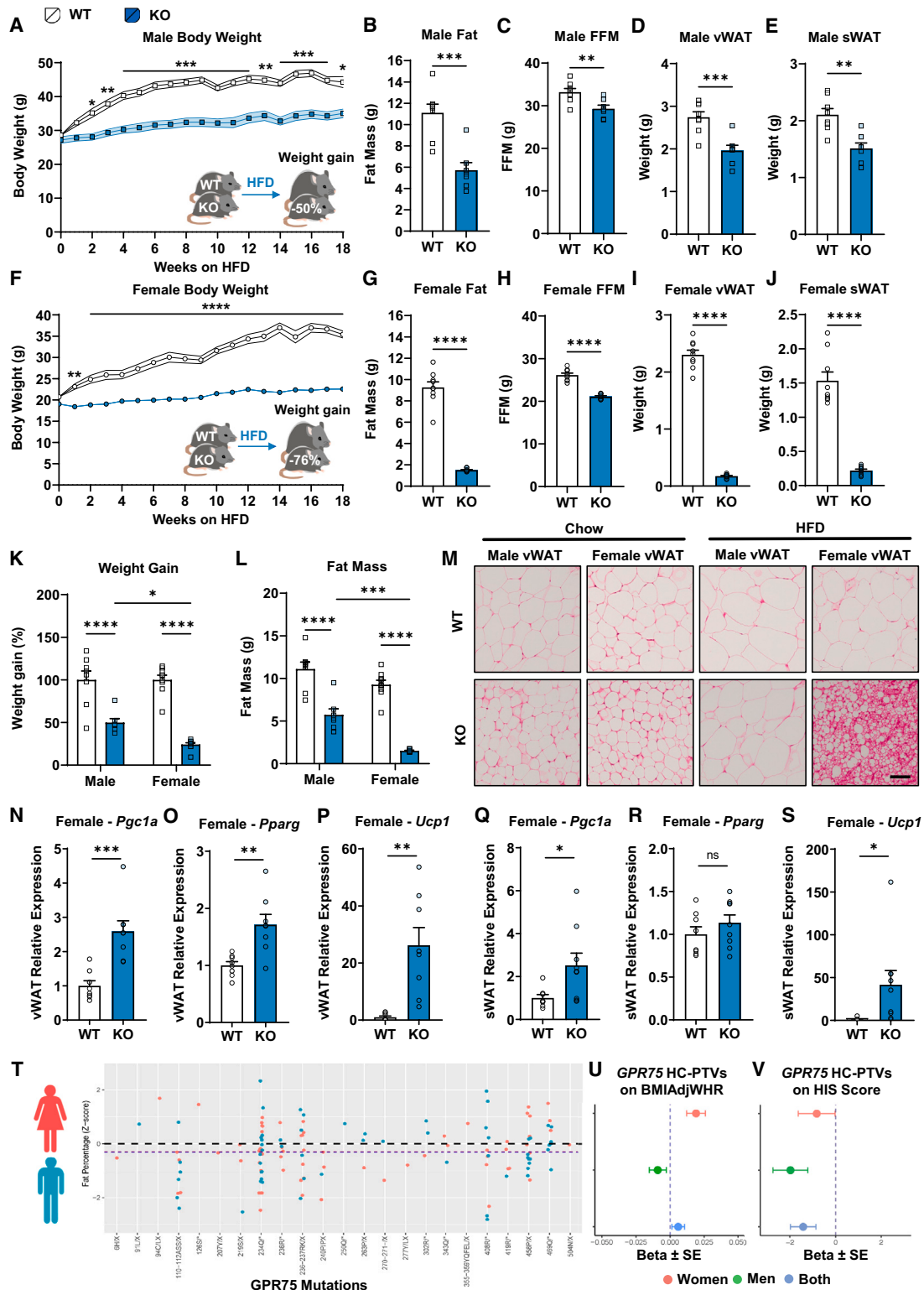


**Figure 3. Loss of *Gpr75* is associated with lower adiposity in mice and humans**

Mice were provided with a 42% high-fat diet (HFD) for 4.5 months.

(A–E) (A) Male *Gpr75* knockout (KO) mice show a significant protection from weight gain (time × genotype  $F_{(18, 284)} = 14.70$ ,  $p < 0.0001$ ) and significantly lower (B) fat mass (DEXA) ( $t(13) = 4.921$ ,  $p = 0.0003$ ), (C) fat-free mass (DEXA) ( $t$  test,  $t(13) = 3.233$ ,  $p = 0.006$ ), (D) dissected visceral white adipose tissue (vWAT)

(legend continued on next page)

rate (MMR; lowest 20 min over 72 h of measurement) was significantly related to lean body mass but was not affected by sex or genotype (Figure S2E). In female mice, the ratio of measured metabolic rate/MMR showed the expected large effect of light vs. dark cycle with more energy expenditure in the dark cycle as compared with light cycle (Figure S2F). In addition, there was a large effect of genotype with female *Gpr75* KO mice having higher energy expenditure compared with WT mice both in the light and dark cycles (Figure S2J). This effect did not reach statistical significance in male mice (Figure S2G); however, the small increase in energy expenditure associated with a significant increase in physical activity could still be physiologically meaningful (Figures S2H and S2I). Further statistical analysis revealed a more pronounced physically active phenotype in female *Gpr75* KO mice as compared with male *Gpr75* KO mice (Figure S2M). We also observed a significant cycle (light vs. dark) by genotype interaction, with the increase in energy expenditure during the dark phase greater in female *Gpr75* KO compared with the WT mice (Figure S2J). These data indicate that HFD-fed *Gpr75* KO mice are more physically active in the dark phase compared with WT mice, consistent with their higher energy expenditure relative to resting levels during the dark cycle.

### ***Gpr75* KO mice have less body fat, and the effect is more prominent in females**

Given that *Gpr75* KO mice maintained on a standard chow diet showed similar levels of caloric intake and energy expenditure relative to WT mice, we expected to observe minor genotypic differences in adiposity on this diet. To test this, body weight and body fat were tracked for 4.5 months in mice fed a standard chow diet. Although chow-fed male *Gpr75* KO mice had comparable body weight to WT mice and female *Gpr75* KO mice had modestly lower body weight compared with WT mice, a large effect on body fat was observed (Figures S3A–S3P). Specifically, male and female chow-fed *Gpr75* KO mice showed significantly lower overall fat mass, which was evident when analyzing both visceral and subcutaneous fat pads (Figures S3A–S3P).

We next investigated the effect of a western 42% HFD on body weight and lipid accumulation over 4.5 months in our novel CRISPR-Cas9 *Gpr75* KO mice. Male *Gpr75* KO mice gained

50% less weight and female *Gpr75* KO mice gained 76% less weight compared with HFD-induced body weight gain in WT mice (Figures 3A and 3F). Similarly, male *Gpr75* KO mice gained 35% less fat mass and female mice gained 74% less fat mass on an HFD as compared with WTs (Figures 3B, 3G, and S3Q–S3V). The reduction in body fat was found in both visceral and subcutaneous adipose tissue depots (Figures 3D, 3E, 3I, and 3J). A sex comparison revealed that HFD-fed female *Gpr75* KO mice gained significantly less body weight and body fat as compared with male *Gpr75* KO mice (Figures 3K and 3L). Histological analysis of visceral fat revealed a striking change in adipocytes in female HFD-fed *Gpr75* KO mice that was not evident in female chow-fed mice or male HFD or chow-fed mice (Figure 3M). Specifically, female HFD-fed *Gpr75* KO mice white adipose tissue had histological browning characteristics that were supported by qPCR analyses (Figures 3M–3S). However, no differences in brown adipose tissue were detected in *Gpr75* KO mice compared with WTs (Figures S4B, S4E, and S4F). Consistent with the histological profile, no changes in thermogenic markers were observed in male HFD-fed *Gpr75* KO mice compared with WT mice (Figures S4C and S4D). Additional body composition analysis revealed that female *Gpr75* KO mice had higher bone mineral content and density relative to WT mice (Figures S4H and S4J). These data illustrate that perturbations in *Gpr75* function protect both male and female mice from gaining body fat and that this phenotype is retained even in the presence of a high-calorie diet and is more pronounced in female mice.

### **Effects of human *GPR75* LOF variants in humans**

A recent publication reported that *GPR75* loss-of-function (LOF) variants are associated with lower BMI and total body fat in 645,626 people (including the UK Biobank [UKBB]).<sup>7</sup> We hypothesized that *GPR75* may have a sex dimorphic effect on body fat deposition, as seen in our mouse model. To test this, we used the publicly available UKBB exomes comprising of 428,719 individuals of European ancestry, where we identified 145 individuals (68 males and 77 females) carrying LOF variants in the coding region of *GPR75* (STAR Methods). First, we confirmed that *GPR75* LOF carriers have a lower percentage of total body fat compared with non-carriers in this group

(t(13) = 4.329,  $p = 0.0008$ ), and (E) dissected subcutaneous white adipose tissue (sWAT) (t(13) = 4.066,  $p = 0.001$ ) weights compared with wild-type (WT) mice ( $n = 7$  per group).

(F–J) (F) Female *Gpr75* KO mice also show a significant protection from weight gain (time  $\times$  genotype  $F_{(18, 288)} = 36.65$ ,  $p < 0.0001$ ) and significantly lower (G) fat mass (DEXA) (t(16) = 14.79,  $p < 0.0001$ ), (H) fat-free mass (DEXA) (t(16) = 10.14,  $p < 0.0001$ ), (I) dissected vWAT (t(16) = 26.16,  $p < 0.0001$ ), and (J) dissected sWAT weights (t(16) = 10.23,  $p < 0.0001$ ) compared with WT mice ( $n = 9$  per group).

(K and L) Female *Gpr75* KO mice show significantly lower HFD-induced (K) percentage weight gain (sex  $\times$  genotype  $F_{(1, 29)} = 4.148$ ,  $p = 0.05$ ) and (L) fat mass (sex  $\times$  genotype  $F_{(1, 29)} = 4.290$ ,  $p = 0.04$ ) compared with male *Gpr75* KO mice.

(M–S) (M) Fat-soluble dye Oil Red O histology of male and female vWAT on chow diet and following 4.5 months HFD feeding in *Gpr75* KO and WT mice. Scale bar, 100  $\mu\text{m}$ . Female *Gpr75* KO mice have increased qPCR mRNA expression of lipid metabolism and energy expenditure markers *Pgc1a* (vWAT t(14) = 4.616,  $p = 0.0004$ , sWAT t(15) = 2.443,  $p = 0.03$ ), *Pparg* (vWAT t(14) = 3.711,  $p = 0.002$ , sWAT t(15) = 1.048,  $p = 0.3$ ), and *Ucp1* (vWAT t(14) = 4.015,  $p = 0.001$ , sWAT t(15) = 2.282,  $p = 0.04$ ) in (N)–(P) vWAT and (Q)–(S) sWAT compared with WT mice.

(T) Whole exome analysis of 428,719 individuals from UK Biobank dataset analyzing association between *GPR75* variants and body fat identified 135 individuals (female:  $n = 72$ ; male:  $n = 63$ ) carrying high-confidence (HC) protein-truncating variants (PTVs) in *GPR75*. Distribution plot shows percentage body fat score (Z score) calculated by sex against HC PTV mutations. An association between HC PTV *GPR75* mutations and lower fat percentage was observed overall (combined: Bolt-Imm Inf  $p = 0.0016$ , beta =  $-1.5906$ , SE = 0.5038, STAAR-O  $p = 0.0027$ ) and when examining males (blue line; STAAR-O  $p = 0.0364$ , Bolt-Imm Inf  $p = 0.011$ , beta =  $-1.7294$ , SE = 0.6760) and females (red line; Bolt-Imm Inf  $p = 0.016$ , beta =  $-1.7998$ , SE = 0.7503, STAAR-O  $p = 0.0363$ ) separately.

(U) Forest plot showing effect of *GPR75* HC PTVs on waist-hip ratio adjusted for BMI (BMIAdjWHR) indicating a significant sex difference. (Combined beta  $\pm$  SE = 0.0060  $\pm$  0.0047,  $p = 0.2$ ; female beta  $\pm$  SE = 0.0191  $\pm$  0.0068,  $p = 0.0052$ ; male beta  $\pm$  SE =  $-0.0090 \pm 0.0063$ ,  $p = 0.15$ ;  $p$  diff (male vs. female) = 0.0024.)

(V) Forest plot showing effect of *GPR75* HC PTVs on hepatic steatosis index (HSI), illustrating *GPR75* HC PTVs have a lower rating compared with non-carriers (combined beta  $\pm$  SE = 1.42  $\pm$  0.559,  $p = 0.012$ ). \* $p < 0.05$ , \*\* $p < 0.01$ , \*\*\* $p < 0.001$ , \*\*\*\* $p < 0.0001$ .

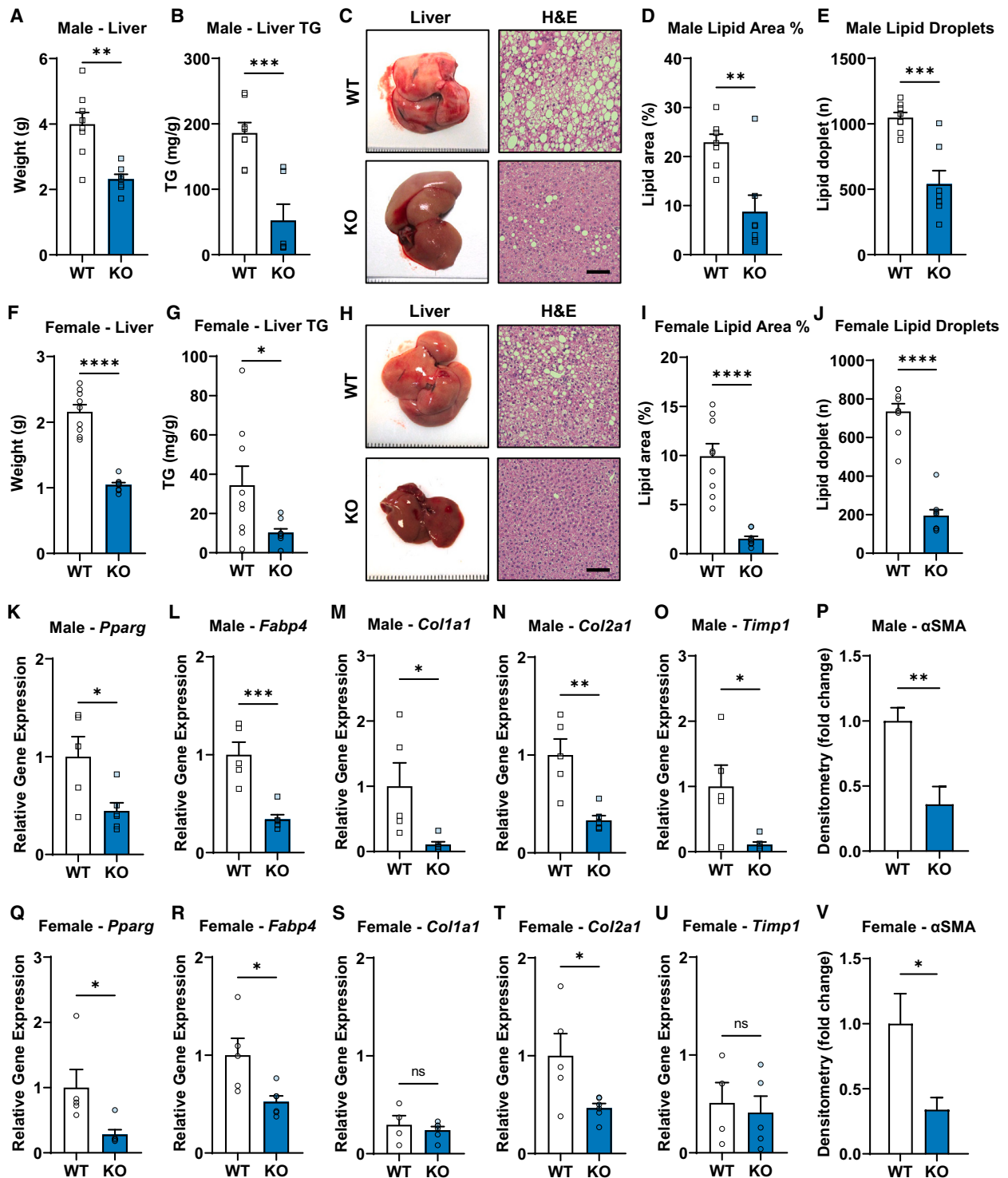


**Figure 4. *Gpr75* knockout mice are protected from fatty liver**

(A–E) Male *Gpr75* knockout (KO) mice show (A) lower dissected liver weight ( $t(13) = 4.132, p = 0.001$ ), (B) liver triglyceride content ( $t(12) = 4.750, p = 0.0005$ ), (C and D) lower lipid percentage ( $t(13) = 3.943, p = 0.002$ ), and (C and E) number of lipid droplets ( $t(13) = 4.855, p = 0.0003$ ) compared with and wild-type (WT) mice fed HFD for 4.5 months. Scale bars, 100  $\mu$ m.

(F–J) Similarly, female *Gpr75* KO mice show (F) lower dissected liver weight ( $t(16) = 9.823, p < 0.0001$ ), (G) liver triglyceride content ( $t(16) = 2.432, p = 0.03$ ), (H and I) lower lipid percentage ( $t(16) = 6.472, p < 0.0001$ ), and (H and J) number of lipid droplets ( $t(16) = 10.74, p < 0.0001$ ) compared with WT mice fed HFD for 4.5 months. Scale bars, 100  $\mu$ m.

(legend continued on next page)

(beta  $\pm$  SE =  $-1.5906\% \pm 0.5038\%$ ,  $p = 0.0016$ ). Next, we examined total percent body fat by sex and observed no differences associated with specific *GPR75* mutations or degree of percent body fat associated with male and female *GPR75* LOF carriers (Figures 3T, S4L, and S4M; Tables S1B–S1F; male beta  $\pm$  SE =  $-1.7294\% \pm 0.6760\%$ ,  $p = 0.011$ ; female beta  $\pm$  SE =  $-1.7998\% \pm 0.7503\%$ ,  $p = 0.016$ ; male vs. female  $p = 0.9406$ ). However, when we examined the effect of *GPR75* LOFs on body fat distribution using waist-hip ratio (WHR) as a proxy, *GPR75* LOF variants were associated with higher WHR in women after adjusting for BMI, and this effect was absent in men (Figure 3U; Table S1C; combined beta  $\pm$  SE =  $0.0060 \pm 0.0047$ ,  $p = 0.2$ ; female beta  $\pm$  SE =  $0.0191 \pm 0.0068$ ,  $p = 0.0052$ ; male beta  $\pm$  SE =  $-0.0090 \pm 0.0063$ ,  $p = 0.15$ ;  $p$  male vs. female =  $0.0024$ ). This implies that *GPR75* LOFs may affect the deposition of lipid in humans in a sex-dependent manner.

To date, the majority of genes whose disruption promotes leanness in people lead to forms of lipodystrophy. This disease impairs the safe storage of lipids in adipocytes, which promotes harmful lipid accumulation in other tissues, particularly the liver. We next asked if *GPR75* LOF variants protect against or promote non-alcoholic liver disease (NALD). However, the rarity of *GPR75* LOF variants, coupled with the well-known healthy participant bias of the UKBB,<sup>18</sup> resulted in a nonrepresentative low prevalence of NALD in the UKBB compared with other cohorts,<sup>19</sup> thereby hindering the direct analysis of the disease. Therefore, we examined the effect via liver function tests: blood alanine transaminase (ALT) and aspartate aminotransferase (AST) levels and the hepatic steatosis index (HSI =  $8 \times \text{ALT}/\text{AST} + \text{BMI}$  [+2 if type 2 diabetes yes, +2 if female]) developed to determine the likelihood of hepatic steatosis.<sup>20–22</sup> Though *GPR75* LOF carriers have indistinguishable blood ALT ( $p = 0.346$ ) and AST ( $p = 0.715$ ) levels compared with the non-carriers (Figures S4N and S4O), they do display a BMI-dependent lower HSI score (beta  $\pm$  SE =  $-1.42 \pm 0.559$ ,  $p = 0.012$ ) (Figure 3V). These results imply that *GPR75* LOF carriers have a reduced risk of lipid accumulation in liver. We next utilized *Gpr75* KO mice to further investigate the protective effect of *GPR75* mutations on liver disease in appropriately powered studies.

### ***Gpr75* KO mice are protected from developing NAFLD**

To investigate the effect of *GPR75* on NAFLD, *Gpr75* KO and WT mice were fed an HFD for 4.5 months, and liver health was evaluated by analysis of lipid content, markers of lipid storage, and fibrosis. Both male and female *Gpr75* KO mice livers weighed less and had reduced triglyceride and lipid percentage (Figures 4A–4J). A sex difference was not observed in the protective effect of *Gpr75* KO mice on liver lipid accumulation (Figure S4K). The lower hepatic triglyceride content and lipid percentage in the *Gpr75* KO mice corresponded to lower expres-

sion of lipid droplet storage markers (peroxisome proliferator-activated receptor gamma [PPAR $\gamma$ ] and fatty acid binding protein 4 [Fabp4]; Figures 4K, 4L, 4Q, and 4R). *Gpr75* KO mice also had reduced expression of extracellular matrix markers (collagen 1, collagen 2, tissue inhibitor of metalloproteinase 1 [TIMP1], and  $\alpha$ SMA), indicating less HFD-induced liver fibrosis compared with WT mice (Figures 4M–4P, 4S–4V, and S4P). These findings support that *Gpr75* loss reduces adipose mass by beneficially altering energy balance rather than by restricting the expansion of adipose tissue as seen in lipodystrophies. These data indicate that both male and female *Gpr75* KO mice are significantly protected from HFD-induced liver lipid accumulation and show a reduction in NAFLD severity compared with WT mice, findings consistent with analysis of *GPR75* LOF carriers from the UKBB.

### **DISCUSSION**

Despite the high global prevalence of NAFLD, there are currently no medications to specifically treat this condition. Here, we identify *GPR75* as a target to significantly reduce lipid accumulation in the liver. *GPR75* genetic variation or deletion was also associated with significantly lower percent body fat in both humans and mice, providing support for this receptor in preventing or reducing lipid accumulation more broadly in conditions such as obesity. Though *GPR75* genetic variation was associated with significantly lower body fat in both males and females, a sex difference was identified in the characteristics of adipose tissue, suggesting that females may show greater benefit from *GPR75* pharmaceutical interventions.

Very few genes that, when mutated, cause healthy leanness have been identified.<sup>7,23</sup> The discovery of *GPR75* is therefore important because *GPR75* variants are associated with the largest decrease in body weight in humans reported to date, reflecting in the UKBB 1.8 kg/m<sup>2</sup> lower BMI (approximately 5.3 kg lower body weight). The magnitude of this gene effect on body weight is on par with the scale of weight gain seen with LOF *MC4R* mutations (1.6 kg/m<sup>2</sup> higher BMI) in UKBB. This indicates that *GPR75* genetic variation is not only associated with the biggest effect on human leanness but also that this gene produces one of the largest effects overall on human adiposity discovered to date.

Our findings indicate that *Gpr75* loss does not lower fat mass by restricting adipose tissue expansion per se. This is important as limiting adipose expansion in the face of overnutrition typically promotes ectopic fat accumulation in liver and worsens metabolic health, as is seen in conditions such as lipodystrophies. Instead, we report that loss of *Gpr75* substantially protects against the development of fatty liver. We performed a more detailed characterization of adiposity in mice and people with *GPR75* LOF variants and uncovered a sex difference. Specifically, HFD-fed female *Gpr75* KO mice showed a greater

(K–O) Liver qPCR expression levels of lipid handling markers (K) peroxisome proliferator-activated receptor gamma (*Pparg*) ( $t(9) = 2.695$ ,  $p = 0.02$ ), (L) fatty acid binding protein 4 (*Fabp4*) ( $t(9) = 5.195$ ,  $p = 0.0006$ ), and fibrosis markers (M) collagen1 (*Col1a1*) ( $t$  test,  $t(9) = 2.736$ ,  $p = 0.02$ ), (N) collagen2 (*Col2a1*) ( $t(9) = 4.253$ ,  $p = 0.002$ ), and (O) TIMP metalloproteinase inhibitor 1 (*Timp1*) ( $t(9) = 2.990$ ,  $p = 0.02$ ).

(P) Western blot quantification of fibrosis marker  $\alpha$ SMA in the liver of HFD-fed male KO mice compared with WT controls ( $t(9) = 3.642$ ,  $p = 0.005$ ).

(Q–V) Similarly, analysis of markers of fibrosis and lipid storage was performed in the liver of *Gpr75* KO female mice compared with WT controls fed an HFD (*Pparg*  $t(9) = 2.728$ ,  $p = 0.02$ ; *Fabp4*  $t(9) = 2.818$ ,  $p = 0.02$ ; *Col1a1*  $t(8) = 0.6292$ ,  $p = 0.5$ ; *Col2a1*  $t(9) = 2.550$ ,  $p = 0.03$ ; *Timp1*  $t(7) = 0.37$ ,  $p = 0.7$ ;  $\alpha$ SMA  $t(9) = 2.847$ ,  $p = 0.02$ ). \* $p < 0.05$ , \*\* $p < 0.01$ , \*\*\* $p < 0.001$ , \*\*\*\* $p < 0.0001$ .

protective effect on lipid accumulation as compared with male *Gpr75* KO mice and evidence of browning in white adipose tissue. The effect on browning appears to be a consequence of the HFD since it was not evident in female *Gpr75* KO mice fed a chow diet. This diet-related physiological effect increasing the thermogenic capacity of white adipose tissue could further the appeal of GPR75 as a pharmaceutical target for obesity treatment. To investigate whether a sex bias in the protective effect of GPR75 on body fat accumulation also exists in people, we examined percent body fat in men and women with and without GPR75 genetic variants in the UKBB. We mapped GPR75 high-confidence (HC) protein-truncating variant (PTV) in both men and women by degree of body fat. The most common variant was 234Q/\*. There was no obvious sex difference in the expression of a particular GPR75 variant. However, a sex difference was observed in WHR with female GPR75 HC PTV carriers tending to have a higher WHR compared with non-carriers, consistent with less fat distributed in the hips. Although this appears counterintuitive, it may be a reflection of greater leanness in the GPR75 HC PTV carriers. A difference in WHR was not observed in male GPR75 HC PTV carriers vs. non-carriers. These data indicate that male and female GPR75 HC PTV and *Gpr75* KO mice are significantly leaner compared with controls, and a sex bias warrants further investigation.

Given the established “healthy skew” of the UKBB<sup>18</sup> and the rarity of LOF GPR75 mutations, only 3 GPR75 mutation carriers met criteria for NAFLD, making it difficult to draw any meaningful conclusions with regards to protection against this disease in the UKBB. Thus, we instead used HSI as a proxy in the UKBB sample and our mouse model for detailed characterization of the role of GPR75 in liver fat accumulation and disease. GPR75 LOF carriers had a lower HSI score, suggesting that they have a reduced risk of lipid accumulation in liver. To evaluate this effect in more detail in appropriately powered studies, we profiled *Gpr75* KO and WT mice. This revealed that HFD-fed *Gpr75* KO mice were significantly protected from the development of fatty liver. Both male and female WT mice fed an HFD for 4.5 months had approximately 40% of their liver as lipid, triglycerides were elevated, and showed a significant increase in markers of fibrosis. By contrast, male and female *Gpr75* KO mice retained healthy livers with very little lipid accumulation. The observation that *Gpr75* KO mice are protected from NAFLD and hepatic steatosis demonstrates that GPR75 is a promising new target for the treatment of NAFLD.

We aimed to establish how the absence of GPR75 produces this protective effect on lipid accumulation. The field is still at the beginning of understanding the expression and function of GPR75, its ligand(s), and signaling pathways. GPR75 is classified as an orphan GPCR by the International Union of Basic and Clinical Pharmacology (IUPAHR). Recently, RANTES and 20-hydroxyeicosatetraenoic acid (20-HETE) have been proposed as ligands for GPR75<sup>24–29</sup>; however, we and others observe constitutive GPR75 Gi- and  $\beta$ -arrestin coupling.<sup>29</sup> GPR75 maps onto chromosome 2p16 and encodes a 540 amino acid long protein and has been reported to be highly expression in the brain, retina, and testes in people.<sup>24,30</sup> We performed a quantitative analysis of the tissue distribution of *Gpr75* in mouse, which also showed the highest expression of *Gpr75* in the brain. We next performed the first detailed map of *Gpr75* brain expres-

sion, which indicated that it is widely expressed throughout the mouse brain. This is in contrast to other genes influencing adiposity, such as *Agrp* and *Pomc*, which are exclusively expressed in small defined subregions of the brain.<sup>11,31</sup> Focusing on the adiposity-related brain region the hypothalamus, we observed that *Gpr75* is heterogeneously expressed, including cells containing various neuropeptides, neurotransmitters, receptors, and genes associated with energy homeostasis, body weight, and body fat regulation. Given the widespread distribution of *Gpr75*, the relative percentage of co-expression with a specific subpopulation of cells is small but could be physiologically meaningful. Illustrating the heterogeneous nature of anatomical hypothalamic expression, cells with the highest expression of *Gpr75* are found in different regions of the hypothalamus. These include ARC NAG neurons, SCN vasoactive intestinal peptide receptor 2 (*Vipr2*) neurons, and mammillary body *Foxb1* neurons.

NAG neurons have been extensively studied for their essential role in appetite and body weight regulation.<sup>11</sup> Npy, *Agrp*, and GABA derived from NAG neurons each control food intake through action at their own second-order neurons.<sup>32–34</sup> Demonstrating the translational relevance of the *Agrp* component of NAG neurons, the MC4R agonist setmelanotide is used to treat genetic forms of extreme obesity.<sup>17</sup> Previous reports indicate that the dynamics of NAG neurons are altered by HFD.<sup>35,36</sup> It is possible that *Gpr75* plays a role in dietary fat action/signaling in NAG neurons, and thereby, in the absence of *Gpr75*, NAG neurons retain the ability to appropriately regulate caloric intake. This is one possible explanation requiring further study for the observation that *Gpr75* KO mice retain equivalent caloric intake when provided with chow or HFD, a response that ultimately prevents HFD-induced weight gain and NAFLD. Here, we demonstrate that *Gpr75* is new player positioned to influence the activity of a subset of key appetite and adiposity-controlling NAG neurons.

*Gpr75* is also co-expressed with *Vipr2*, a receptor necessary for normal circadian rhythms in rest/activity behavior.<sup>37</sup> This suggests that *Gpr75* may play a role in the regulation of circadian rhythms or SCN function. However, *Gpr75* KO mice exhibited broadly normal circadian-related eating and activity behavior. The transcription factor *Foxb1* (formerly known as *Fkh5*) is required for normal CNS development. Specifically, *Foxb1* KO mice suffer substantial perinatal degeneration of the hypothalamic medial and lateral mammillary body in the posterior hypothalamus, a region involved in body temperature and spatial and working memory.<sup>38,39</sup> The gross anatomy of the posterior hypothalamus appeared normal in *Gpr75* KO mice. We believe that the widespread distribution of *Gpr75* within the brain suggests that it likely influences lipid accumulation by acting through more than one brain pathway, analogous to the leptin receptor and 5-HT<sub>2C</sub> receptor<sup>40,41</sup>; however, this remains to be determined. The characterization of *Gpr75*-positive neurons also suggests that *Gpr75* may contribute to other hypothalamic functions. This first detailed characterization of hypothalamic *Gpr75* expression provides a resource for future investigation into the mechanism through which *Gpr75* influences physiology, health, and eating behavior.

We profiled energy homeostasis in *Gpr75* KO mice to clarify how *Gpr75* genetic perturbation protects against lipid accumulation in the liver and more broadly. An earlier study of

*Gpr75* KO mice assessed before sexual maturity reported that young *Gpr75* KO mice are mildly hypophagic on an HFD and have no differences in physical activity or energy expenditure.<sup>9</sup> As we were interested in the function of the receptor in adulthood, here we provide a detailed characterization of energy homeostasis in adult *Gpr75* KO and WT mice. We found no genotypic differences in food intake on a chow diet, indicating that *Gpr75* KO mice are not hypophagic. *Gpr75* KO mice adjusted caloric intake to retain energy balance when provided with an HFD, illustrating that they are adept at calibrating caloric intake to energy demands. We also observed that adult *Gpr75* KO mice did not have altered minimal metabolic rates but were more physically active, and this was associated with an increase in the energy expenditure relative to the MMR on HFD. Consistent with this, a recent paper using a different *Gpr75* KO mouse line reported that adult *Gpr75* KO mice display higher energy expenditure compared with WT mice when provided with an HFD but not when fed a chow diet (physical activity was not measured).<sup>9</sup> We conclude that the protective effect of *Gpr75* genetic inactivation on HFD-associated NAFLD is associated with maintained energy balance that prevents DIO and NAFLD.

Here we report that LOF of *GPR75* significantly protects against the development of liver disease. More broadly, *GPR75* has emerged as a gene producing the strongest association with leanness identified to date in people. This role of *GPR75* in lipid accumulation persists with different diets, and we report that it is related to calibrating energy intake to energy demands to maintain energy balance. This makes *GPR75* an attractive drug target to control adiposity. Our results also uncovered a sex effect on the extent to which lipid accumulation was protected, with female *Gpr75* KO mice fed an HFD being more protected than males, and this effect was likely related to greater physical activity and energy expenditure in females. A sex difference was also found in human *GPR75* HC PTV carriers with regards to WHR. We conclude that *GPR75* has a significant role in influencing lipid accumulation in both liver and adipose tissue and warrants investigation as much-needed new therapy for the treatment of NAFLD.

### Limitations of the study

A limitation of using the UKBB to interrogate the function of *GPR75* is the well-described healthy skew of its participants.<sup>18</sup> This is seen in the lower prevalence of obesity within the cohort, compared with the general population (25.6% vs. 31.5% in men; 23.0% vs. 32.2% in women, respectively), and as a result, the far lower prevalence of relevant comorbidities, including NAFLD. Future more representative studies with a higher prevalence of liver disease will more definitively establish whether human variations in *GPR75* are protective from the development of this disease. Likewise, the greater effect of *Gpr75* gene KO on body fat observed in female mice compared with male mice may also be detected in women vs. men in future studies where the complete loss (as opposed to possible partial loss) of *GPR75* function has been verified, which requires *GPR75* to first be deorphanized. Finally, future systematic exploration of different subpopulations of *GPR75* within the brain will establish their individual contributions to lipid accumulation and broader functions in behavior and physiology.

### STAR★METHODS

Detailed methods are provided in the online version of this paper and include the following:

- KEY RESOURCES TABLE
- RESOURCE AVAILABILITY
  - Lead contact
  - Materials availability
  - Data and code availability
- EXPERIMENTAL MODEL AND STUDY PARTICIPANT DETAILS
  - Animal Models
  - Husbandry and Housing Conditions of Experimental Animals
- METHOD DETAILS
  - Whole exome sequencing
  - Metabolic Assessment and Meal Pattern Analysis
  - Mouse Body Composition
  - Tissue Processing
  - Gene expression
  - Western Blot
  - Histology Analysis
  - Triglyceride assay
  - RNAscope ISH
  - Single cell RNA sequencing
- QUANTIFICATION AND STATISTICAL ANALYSIS
  - Statistical analysis

### SUPPLEMENTAL INFORMATION

Supplemental information can be found online at <https://doi.org/10.1016/j.cmet.2024.03.016>.

### ACKNOWLEDGMENTS

The authors thank Thomas McSkimming, Samuel Bundy, Samriti Juneja, Susan Berry, Tongshuo Hu, Yinan Zhang, and staff within the University of Aberdeen Medical Research Facility and the Microscopy Facility staff for their technical assistance. This research has been conducted using data from UKBB (project number 32974), a major biomedical database. Work was supported by the Biotechnology and Biological Sciences Research Council (BB/R01857X/1 and BB/V016849/1 to L.K.H.; BBSRC Mitigation Fund BB/W510634/1 to A.L.-P., L.K.H., and F.M.; BB/V015869/1 to J.J.R.; and BB/S017593/1 to B.Y.H.L.), the Medical Research Council (MC/PC/15077 to L.K.H. and MC\_UU\_00014/1 to G.S.H.Y.), Wellcome Trust Seed Award (205862/Z/16/Z to F.M.), TENOVUS (G20.09 to F.M. and D.T.), and Wellcome Trust Institutional Strategic Support Fund to the University of Aberdeen (to L.K.H., F.M., and A.L.-P.). C.M. is funded by a BBSRC (Eastbio) CASE 4-year PhD studentship. N.S. is supported by a BBSRC Eastbio PhD studentship. Next-generation sequencing was performed by the IMS Genomics and transcriptomics core facility, which is supported by the MRC (MC\_UU\_00014/5), the Wellcome Trust (208363/Z/17/Z), and the Cancer Research UK Cambridge Institute Genomics Core. G.K.C.D. is funded by a BBSRC CASE 4-year PhD studentship, co-funded by Novo Nordisk.

### AUTHOR CONTRIBUTIONS

L.K.H. designed the experiments with input from F.M., G.S.H.Y., and J.J.R.; F.M. and J.I. created the CRISPR-Cas9-deleted *Gpr75* mouse line with input from A.M.; A.L.-P., C.M., B.Y.H.L., G.K.C.D., N.S., P.B.M.d.M., R.C., K.K., E.J.G., J.R.B.P., F.G., J.R.S., and J.J.R. performed experiments and/or data analysis; D.T. provided reagents and intellectual contributions; and L.K.H. and A.L.-P. wrote the manuscript with input from all other authors.

### DECLARATION OF INTERESTS

E.J.G. and J.R.B.P. are employees of and hold shares in Adrestia Therapeutics.

Received: May 30, 2023  
Revised: November 4, 2023  
Accepted: March 29, 2024  
Published: April 22, 2024

## REFERENCES

- American Liver Foundation (2022). Nonalcoholic fatty liver disease (NAFLD). <https://liverfoundation.org/for-patients/about-the-liver/diseases-of-the-liver/non-alcoholic-fatty-liver-disease/>.
- Polyzos, S.A., Kountouras, J., and Mantzoros, C.S. (2019). Obesity and nonalcoholic fatty liver disease: from pathophysiology to therapeutics. *Metabolism* 92, 82–97. <https://doi.org/10.1016/j.metabol.2018.11.014>.
- National Institute of Diabetes and Digestive and Kidney Diseases (2022). Definition & facts of NAFLD & NASH. <https://www.niddk.nih.gov/health-information/liver-disease/naflid-nash/definition-facts>.
- Klein, S., Gastaldelli, A., Yki-Järvinen, H., and Scherer, P.E. (2022). Why does obesity cause diabetes? *Cell Metab.* 34, 11–20. <https://doi.org/10.1016/j.cmet.2021.12.012>.
- Rinella, M.E., and Sanyal, A.J. (2016). Management of NAFLD: a stage-based approach. *Nat. Rev. Gastroenterol. Hepatol.* 13, 196–205. <https://doi.org/10.1038/nrgastro.2016.3>.
- Wing, R.R., and Phelan, S. (2005). Long-term weight loss maintenance. *Am. J. Clin. Nutr.* 82, 222S–225S. <https://doi.org/10.1093/ajcn/82.1.222S>.
- Akbari, P., Gilani, A., Sosina, O., Kosmicki, J.A., Khramian, L., Fang, Y.Y., Persaud, T., Garcia, V., Sun, D., Li, A., and Mbatchou, J. (2021). Sequencing of 640,000 exomes identifies GPR75 variants associated with protection from obesity. *Science* 373, eabf8683. <https://doi.org/10.1126/science.abf8683>.
- Powell, D.R., Doree, D.D., DaCosta, C.M., Platt, K.A., Brommage, R., Buhning, L., Revelli, J.P., and Shadoan, M.K. (2022). Mice lacking Gpr75 are hypophagic and thin. *Diabetes Metab. Syndr. Obes.* 15, 45–58. <https://doi.org/10.2147/DMSO.S342799>.
- Hossain, S., Gilani, A., Pascale, J., Villegas, E., Diegisser, D., Agostinucci, K., Kulaprazhazhe, M.M., Dirice, E., Garcia, V., and Schwartzman, M.L. (2023). Gpr75-deficient mice are protected from high-fat diet-induced obesity. *Obesity (Silver Spring)* 31, 1024–1037. <https://doi.org/10.1002/oby.23692>.
- Steuernagel, L., Lam, B.Y.H., Klemm, P., Dowsett, G.K.C., Bauder, C.A., Tadross, J.A., Hitschfeld, T.S., del Rio Martin, A., Chen, W., de Solis, A.J., et al. (2022). HypoMap – a unified single cell gene expression atlas of the murine hypothalamus. *Nat. Metab.* 4, 1402–1419. <https://doi.org/10.1038/s42255-022-00657-y>.
- Heisler, L.K., and Lam, D.D. (2017). An appetite for life: brain regulation of hunger and satiety. *Curr. Opin. Pharmacol.* 37, 100–106. <https://doi.org/10.1016/j.coph.2017.09.002>.
- Aponte, Y., Atasoy, D., and Sternson, S.M. (2011). AGRP neurons are sufficient to orchestrate feeding behavior rapidly and without training. *Nat. Neurosci.* 14, 351–355. <https://doi.org/10.1038/nn.2739>.
- Krashes, M.J., Koda, S., Ye, C., Rogan, S.C., Adams, A.C., Cusher, D.S., Maratos-Flier, E., Roth, B.L., and Lowell, B.B. (2011). Rapid, reversible activation of AgRP neurons drives feeding behavior in mice. *J. Clin. Invest.* 121, 1424–1428. <https://doi.org/10.1172/JCI46229>.
- Gropp, E., Shanabrough, M., Borok, E., Xu, A.W., Janoschek, R., Buch, T., Plum, L., Balthasar, N., Hampel, B., Waisman, A., et al. (2005). Agouti-related peptide-expressing neurons are mandatory for feeding. *Nat. Neurosci.* 8, 1289–1291. <https://doi.org/10.1038/nn1548>.
- Wu, Q., Howell, M.P., Cowley, M.A., and Palmiter, R.D. (2008). Starvation after AgRP neuron ablation is independent of melanocortin signaling. *Proc. Natl. Acad. Sci. USA* 105, 2687–2692. <https://doi.org/10.1073/pnas.0712062105>.
- Heisler, L.K., Jobst, E.E., Sutton, G.M., Zhou, L., Borok, E., Thornton-Jones, Z., Liu, H.Y., Zigman, J.M., Balthasar, N., Kishi, T., et al. (2006). Serotonin reciprocally regulates melanocortin neurons to modulate food intake. *Neuron* 51, 239–249. <https://doi.org/10.1016/j.neuron.2006.06.004>.
- Clément, K., van den Akker, E., Argente, J., Bahm, A., Chung, W.K., Connors, H., De Waele, K., Farooqi, I.S., Gonneau-Lejeune, J., Gordon, G., et al. (2020). Efficacy and safety of setmelanotide, an MC4R agonist, in individuals with severe obesity due to LEPR or POMC deficiency: single-arm, open-label, multicentre, phase 3 trials. *Lancet Diabetes Endocrinol.* 8, 960–970. [https://doi.org/10.1016/S2213-8587\(20\)30364-8](https://doi.org/10.1016/S2213-8587(20)30364-8).
- Fry, A., Littlejohns, T.J., Sudlow, C., Doherty, N., Adamska, L., Sprosen, T., Collins, R., and Allen, N.E. (2017). Comparison of sociodemographic and health-related characteristics of UK Biobank participants with those of the general population. *Am. J. Epidemiol.* 186, 1026–1034. <https://doi.org/10.1093/aje/kwx246>.
- Verweij, N., Haas, M.E., Nielsen, J.B., Sosina, O.A., Kim, M., Akbari, P., De, T., Hindy, G., Bovijn, J., Persaud, T., et al. (2022). Germline mutations in CIDEB and protection against liver disease. *N. Engl. J. Med.* 387, 332–344. <https://doi.org/10.1056/NEJMoa2117872>.
- Lee, J.H., Kim, D., Kim, H.J., Lee, C.H., Yang, J.I., Kim, Y.J., Yoon, J.H., Cho, S.H., Sung, M.W., and Lee, H.S. (2010). Hepatic steatosis index: a simple screening tool reflecting nonalcoholic fatty liver disease. *Dig. Liver Dis.* 42, 503–508. <https://doi.org/10.1016/j.dld.2009.08.002>.
- Fedchuk, L., Nascimbeni, F., Pais, R., Charlotte, F., Housset, C., and Ratzliff, V.; LIDO Study Group (2014). Performance and limitations of steatosis biomarkers in patients with nonalcoholic fatty liver disease. *Aliment. Pharmacol. Ther.* 40, 1209–1222. <https://doi.org/10.1111/apt.12963>.
- Sviklâne, L., Olmane, E., Dzërve, Z., Kupčs, K., Pirāgs, V., and Sokolovska, J. (2017). Fatty liver index and hepatic steatosis index predict non-alcoholic fatty liver disease in type 1 diabetes. *J. Gastroenterol. Hepatol.* 33, 270–276. <https://doi.org/10.1111/jgh.13814>.
- Yeo, G.S., and Heisler, L.K. (2012). Unraveling the brain regulation of appetite: lessons from genetics. *Nat. Neurosci.* 15, 1343–1349. <https://doi.org/10.1038/nn.3211>.
- Ignatov, A., Robert, J., Gregory-Evans, C., and Schaller, H.C. (2006). RANTES stimulates Ca<sup>2+</sup> mobilization and inositol trisphosphate (IP<sub>3</sub>) formation in cells transfected with G protein-coupled receptor 75. *Br. J. Pharmacol.* 149, 490–497. <https://doi.org/10.1038/sj.bjp.0706909>.
- Dedoni, S., Campbell, L.A., Harvey, B.K., Avdoshina, V., and Mocchetti, I. (2018). The orphan G-protein-coupled receptor 75 signaling is activated by the chemokine CCL5. *J. Neurochem.* 146, 526–539. <https://doi.org/10.1111/jnc.14463>.
- Davenport, A.P., Alexander, S.P., Sharman, J.L., Pawson, A.J., Benson, H.E., Monaghan, A.E., Liew, W.C., Mpamhanga, C.P., Bonner, T.I., Neubig, R.R., et al. (2013). International union of basic and clinical pharmacology. LXXXVIII. G protein-coupled receptor list: recommendations for new pairings with cognate ligands. *Pharmacol. Rev.* 65, 967–986. <https://doi.org/10.1124/pr.112.007179>.
- Southern, C., Cook, J.M., Neetoo-Isseljee, Z., Taylor, D.L., Kettleborough, C.A., Merritt, A., Bassoni, D.L., Raab, W.J., Quinn, E., Wehrman, T.S., et al. (2013). Screening  $\beta$ -arrestin recruitment for the identification of natural ligands for orphan G-protein-coupled receptors. *J. Biomol. Screen.* 18, 599–609. <https://doi.org/10.1177/1087057113475480>.
- Pascale, J.V., Park, E.J., Adebesin, A.M., Falck, J.R., Schwartzman, M.L., and Garcia, V. (2021). Uncovering the signalling, structure and function of the 20-HETE-GPR75 pairing: identifying the chemokine CCL5 as a negative regulator of GPR75. *Br. J. Pharmacol.* 178, 3813–3828. <https://doi.org/10.1111/bph.15525>.
- Lu, S., Jang, W., Inoue, A., and Lambert, N.A. (2021). Constitutive G protein coupling profiles of understudied orphan GPCRs. *PLoS One* 16, e0247743. <https://doi.org/10.1371/journal.pone.0247743>.
- Tarttelin, E.E., Kirschner, L.S., Bellingham, J., Baffi, J., Taymans, S.E., Gregory-Evans, K., Csaky, K., Stratakis, C.A., and Gregory-Evans, C.Y. (1999). Cloning and characterization of a novel orphan G-protein-coupled receptor localized to human chromosome 2p16. *Biochem. Biophys. Res. Commun.* 260, 174–180. <https://doi.org/10.1006/bbrc.1999.0753>.

31. Wu, Q., Boyle, M.P., and Palmiter, R.D. (2009). Loss of GABAergic signaling by AgRP neurons to the parabrachial nucleus leads to starvation. *Cell* *137*, 1225–1234. <https://doi.org/10.1016/j.cell.2009.04.022>.
32. Chen, Y., Essner, R.A., Kosar, S., Miller, O.H., Lin, Y.C., Mesgarzadeh, S., and Knight, Z.A. (2019). Sustained NPY signaling enables AgRP neurons to drive feeding. *eLife* *8*, e46348. <https://doi.org/10.7554/eLife.46348>.
33. Engström Ruud, L., Pereira, M.M.A., de Solis, A.J., Fenselau, H., and Brüning, J.C. (2020). NPY mediates the rapid feeding and glucose metabolism regulatory functions of AgRP neurons. *Nat. Commun.* *11*, 442. <https://doi.org/10.1038/s41467-020-14291-3>.
34. Ollmann, M.M., Wilson, B.D., Yang, Y.K., Kerns, J.A., Chen, Y., Gantz, I., and Barsh, G.S. (1997). Antagonism of central melanocortin receptors in vitro and in vivo by agouti-related protein. *Science* *278*, 135–138. <https://doi.org/10.1126/science.278.5335.135>.
35. Beutler, L.R., Corpuz, T.V., Ahn, J.S., Kosar, S., Song, W., Chen, Y., and Knight, Z.A. (2020). Obesity causes selective and long-lasting desensitization of AgRP neurons to dietary fat. *eLife* *9*, e55909. <https://doi.org/10.7554/eLife.55909>.
36. Qi, Y., Lee, N.J., Ip, C.K., Enriquez, R., Tasan, R., Zhang, L., and Herzog, H. (2023). *Agrp*-negative arcuate NPY neurons drive feeding under positive energy balance via altering leptin responsiveness in POMC neurons. *Cell Metab.* *35*, 979–995.e7. <https://doi.org/10.1016/j.cmet.2023.04.020>.
37. Harmar, A.J., Marston, H.M., Shen, S., Spratt, C., West, K.M., Sheward, W.J., Morrison, C.F., Dorin, J.R., Piggins, H.D., Reubi, J.C., et al. (2002). The VPAC2 receptor is essential for circadian function in the mouse suprachiasmatic nuclei. *Cell* *109*, 497–508. [https://doi.org/10.1016/S0092-8674\(02\)00736-5](https://doi.org/10.1016/S0092-8674(02)00736-5).
38. Wehr, R., Mansouri, A., de Maeyer, T., and Gruss, P. (1997). *Fkh5*-deficient mice show dysgenesis in the caudal midbrain and hypothalamic mammillary body. *Development* *124*, 4447–4456. <https://doi.org/10.1242/dev.124.22.4447>.
39. Radyushkin, K., Anokhin, K., Meyer, B.I., Jiang, Q., Alvarez-Bolado, G., and Gruss, P. (2005). Genetic ablation of the mammillary bodies in the *Foxb1* mutant mouse leads to selective deficit of spatial working memory. *Eur. J. Neurosci.* *21*, 219–229. <https://doi.org/10.1111/j.1460-9568.2004.03844.x>.
40. Pan, W.W., and Myers, M.G., Jr. (2018). Leptin and the maintenance of elevated body weight. *Nat. Rev. Neurosci.* *19*, 95–105. <https://doi.org/10.1038/nrn.2017.168>.
41. D'Agostino, G., Lyons, D., Cristiano, C., Lettieri, M., Olarte-Sanchez, C., Burke, L.K., Greenwald-Yarnell, M., Cansell, C., Doslikova, B., Georgescu, T., et al. (2018). Nucleus of the solitary tract serotonin 5-HT<sub>2C</sub> receptors modulate food intake. *Cell Metab.* *28*, 619–630.e5. <https://doi.org/10.1016/j.cmet.2018.07.017>.
42. Gardner, E.J., Kentistou, K.A., Stankovic, S., Lockhart, S., Wheeler, E., Day, F.R., Kerrison, N.D., Wareham, N.J., Langenberg, C., O'rahilly, S., et al. (2022). Damaging missense variants in *IGF1R* implicate a role for IGF-1 resistance in the etiology of type 2 diabetes. *Cell Genom.* *2*, 100208. <https://doi.org/10.1016/j.xgen.2022.100208>.
43. Hao, Y., Hao, S., Andersen-Nissen, E., Mauck, W.M., 3<sup>rd</sup>, Zheng, S., Butler, A., Lee, M.J., Wilk, A.J., Darby, C., Zager, M., et al. (2021). Integrated analysis of multimodal single-cell data. *Cell* *184*, 3573–3587.e29. <https://doi.org/10.1016/j.cell.2021.04.048>.
44. Arganda-Carreras, I., Kaynig, V., Rueden, C., Eliceiri, K.W., Schindelin, J., Cardona, A., and Sebastian Seung, H. (2017). Trainable Weka Segmentation: a machine learning tool for microscopy pixel classification. *Bioinformatics* *33*, 2424–2426. <https://doi.org/10.1093/bioinformatics/btx180>.
45. van den Pol, A.N., Yao, Y., Fu, L.Y., Foo, K., Huang, H., Coppari, R., Lowell, B.B., and Broberger, C. (2009). Neuromedin B and gastrin-releasing peptide excite arcuate nucleus neuropeptide Y neurons in a novel transgenic mouse expressing strong Renilla green fluorescent protein in NPY neurons. *J. Neurosci.* *29*, 4622–4639. <https://doi.org/10.1523/JNEUROSCI.3249-08.2009>.
46. Goebel, M., Stengel, A., Wang, L., and Taché, Y. (2011). Central nesfatin-1 reduced the nocturnal food intake in mice by reducing meal size and increasing inter-meal intervals. *Peptides* *32*, 36–43. <https://doi.org/10.1016/j.peptides.2010.09.027>.
47. Johnston, S.L., Peacock, W.L., Bell, L.M., Lonchampt, M., and Speakman, J.R. (2005). PIXImus DXA with different software needs individual calibration to accurately predict fat mass. *Obes. Res.* *13*, 1558–1565. <https://doi.org/10.1038/oby.2005.191>.

## STAR★METHODS

### KEY RESOURCES TABLE

REAGENT or RESOURCE	SOURCE	IDENTIFIER
<b>Antibodies</b>		
Anti-alpha smooth muscle Actin antibody (Goat, polyclonal)	Abcam	Cat# ab21027; RRID: AB_1951138
B-Tubulin (D3U1W) Mouse	Cell Signaling	Cat# 86298; RRID: AB_2715541
Anti-mouse IgG HRP-linked secondary	Cell Signaling	Cat# 7076; RRID: AB_330924
Rabbit Anti-Goat IgG H&L	Abcam	Cat# ab6697; RRID: AB_955988
<b>Biological samples</b>		
Tissue collected from Gpr75 WT and Knockout mice	This paper	N/A
<b>Chemicals, peptides, and recombinant proteins</b>		
Hematoxylin Solution, Gill No. 3	Sigma-Aldrich	Cat# GHS316
Formalin solution, neutral buffered, 10%	Sigma-Aldrich	Cat# HT501320
<b>Critical commercial assays</b>		
RNeasy Mini Kit	QIAGEN	Cat# 74106
M-MLV Reverse Transcriptase	Invitrogen	Cat# 28025013
PowerSYBR Green PCR Master Mix	Applied Biosystems	Cat# 4367659
Pierce BCA Protein Assay Kit	ThermoScientific	Cat# 23227
Triglyceride Liquid Assay	Sentinel Diagnostics	Cat# 17624H
RNAscope 2.5 HD Assay Detection – Brown	Advanced Cell Diagnostics	Cat# 322310
RNAscope Gpr75 Probe	Advanced Cell Diagnostics	Cat# 318281
<b>Deposited data</b>		
UK Biobank (exome sequencing data). Project number 32974.	UK Biobank	<a href="http://www.ukbiobank.ac.uk">www.ukbiobank.ac.uk</a>
HypoMap – single cell gene expression atlas of the murine hypothalamus	Steuernagel et al. <sup>10</sup>	<a href="https://doi.org/10.1038/s42255-022-00657-y">https://doi.org/10.1038/s42255-022-00657-y</a>
Single-cell RNA-seq data from HypoMap.	Cambridge Repository, CELLxGENE, GEO: GSE132355, GSE193921, GSE132730, GSE207736, GSE113576, GSE172204, SRP135960, GSE167927, GSE172461, GSE130597, GSE132608, GSE119960, GSE93374, GSE125065, GSE117295, GSE146692, GSE87544	<a href="https://doi.org/10.17863/CAM.87955">https://doi.org/10.17863/CAM.87955</a> , <a href="https://cellxgene.cziscience.com/collections/d86517f0-fa7e-4266-b82e-a521350d6d36">https://cellxgene.cziscience.com/collections/d86517f0-fa7e-4266-b82e-a521350d6d36</a>
<b>Experimental models: Organisms/strains</b>		
Mouse: Gpr75 knockout mouse	This paper	N/A
Mouse: B6.FVB-Tg(Npy-hrGFP)1Lowl/J	The Jackson Laboratory	JAX: 006417
<b>Oligonucleotides</b>		
CRISPR SG-GPR75 FW 5'-CACCGT GCTATTTCCCCCGTGACG-3'	This paper	N/A
CRISPR SG-GRP75 RV 5'-AAACCTG CACGGGGGAAATAGCAC-3'	This paper	N/A
Collagen 1 FW-5'-CCAAAGGTGCTGATGGTTCT-3'	This paper	N/A
Collagen 1 RV-5'-ACCAGCTTACCCTTGTCAC-3'	This paper	N/A
Collagen 2: FW-5'-CCTCAAGGCAAAGTTGGTCCT-3'	This paper	N/A
Collagen 2: RV-5'-GGCTCCAGGAATACCATCAGT-3'	This paper	N/A
Fabp4: FW-5'- CAAACTGGGCGTGAATTCG-3'	This paper	N/A
Fabp4: RV-5'-ACCAGCTTGTACCATCTCG-3'	This paper	N/A
Gpr75 (5-bp Deletion): FW-5'-TAAACATG CCTCCCCTGCACG-3'	This paper	N/A

(Continued on next page)

**Continued**

REAGENT or RESOURCE	SOURCE	IDENTIFIER
Gpr75 (5-bp Deletion): RV-5'-GATGG CAAGCAGAAAAGTGC-3'	This paper	N/A
Gpr75: FW-5'- TCTTCTTTGGCACATGCTCG-3'	This paper	N/A
Gpr75: RV-5'- CACTGGACGTGAAAAGACGA-3'	This paper	N/A
Hprt: FW-5'- GTTAAGCAGTACAGCCCCAAA-3'	This paper	N/A
Hprt: RV-5'- AGGGCATATCCAACAACAACTT-3'	This paper	N/A
Nono: FW-5'- GCCAGAATGAAGGCTTGACTAT-3'	This paper	N/A
Nono: RV-5'- TATCAGGGGGAAGATTGCCCA-3'	This paper	N/A
Pgc1a: FW-5'- AGCCTCTTTGCCAGATCTT-3'	This paper	N/A
Pgc1a: RV-5'- GGCAATCCGTCTTCATCCAC-3'	This paper	N/A
Pparg: FW-5'-CAGACCTCAGGCAGATCGTC-3'	This paper	N/A
Pparg: RV-5'-GAAGGAACACGTTGTGAGCG-3'	This paper	N/A
TIMP1: FW-5'-GCAACTCGGACCCTGGTCATAA-3'	This paper	N/A
TIMP1: RV-5'-CGCCCCGTGATGAGAACT-3'	This paper	N/A
Ywhaz: FW-5'- GAAAAGTTCTTGATCCCCAATGC-3'	This paper	N/A
Ywhaz: RV-5'- TGTGACTGGTCCACAATTCCTT-3'	This paper	N/A

**Software and algorithms**

Fiji/ImageJ	Schindelin et al.	<a href="https://doi.org/10.1038/nmeth.2019">https://doi.org/10.1038/nmeth.2019</a>
GraphPad Prism Version 9.4	GraphPad	<a href="https://www.graphpad.com/">https://www.graphpad.com/</a>
Research Analysis Platform (UK Biobank Data)	Gardner et al. <sup>42</sup>	<a href="https://doi.org/10.1016/j.xgen.2022.100208">https://doi.org/10.1016/j.xgen.2022.100208</a>
Seurat Package Version 4.0.3/R 4.1	Hao et al. <sup>43</sup>	<a href="https://doi.org/10.1016/j.cell.2021.04.048">https://doi.org/10.1016/j.cell.2021.04.048</a>
Weka Segmentation Tool (ImageJ)	Arganda-Carreras et al. <sup>44</sup>	<a href="https://doi.org/10.1093/bioinformatics/btx180">https://doi.org/10.1093/bioinformatics/btx180</a>

**RESOURCE AVAILABILITY**

**Lead contact**

Further information and requests for resources and reagents should be directed to and will be fulfilled by the lead contact, Lora K. Heisler ([lora.heisler@abdn.ac.uk](mailto:lora.heisler@abdn.ac.uk)).

**Materials availability**

Mouse lines generated in this study are available at request to co-corresponding author, Fiona Murray ([fmurray@abdn.ac.uk](mailto:fmurray@abdn.ac.uk)).

**Data and code availability**

Single-cell RNA-seq data have been deposited at Cambridge Repository and are publicly available. The hypothalamic nucSeq are available in an interactive CellxGene viewer (available via <https://www.mrl.ims.cam.ac.uk>). Additionally, the Seurat object containing the HypoMap is deposited at University of Cambridge's Apollo Repository (<https://doi.org/10.17863/CAM.87955>) in standard RDS format. The source data for the HypoMap can be found CELLxGENE (<https://cellxgene.cziscience.com/collections/d86517f0-fa7e-4266-b82e-a521350d6d36>) accession numbers: GSE132355, GSE193921, GSE132730, GSE207736, GSE113576, GSE172204, SRP135960, GSE167927, GSE172461, GSE130597, GSE132608, GSE119960, GSE93374, GSE125065, GSE117295, GSE146692, GSE87544. All code is publicly available as of the date of publication and DOIs are listed in the [key resources table](#). Details of any additional information required to reanalyze the data reported in this paper is available from the [lead contact](#) upon request. Source data are provided with this paper and all data will be shared by the [lead contact](#) upon request.

**EXPERIMENTAL MODEL AND STUDY PARTICIPANT DETAILS**

**Animal Models**

Adult male and female *Gpr75* KO and WT and *Npy-hrGFP* mice<sup>45</sup> were used. *Gpr75* KO mice were created in house using CRISPR-Cas9. Single guides targeting the early coding region sequence of *Gpr75* were used to introduce a deletion in the protein coding region of *Gpr75* (CRISPR SG-GPR75 FW 5'-CACCGTGCTATTCCCCCGTGAG-3' CRISPR SG-GPR75 RV 5'-AAACCTG CACGGGGGAAATAGCAC-3'). The resulting mouse was sequenced which confirmed an 5bp deletion and introduction of premature

stop codon. Littermates of the same sex were assigned to experimental groups based on their genotype and experiments were carried out in mice between 2–8 months old. Both male and female mice were used for experiments as reported. All procedures were carried out in accordance with the U.K. Animals (Scientific Procedures) Act 1986 and following local ethical approval at University of Aberdeen.

### Husbandry and Housing Conditions of Experimental Animals

Mice were group-housed with *ad libitum* access to food and water in a 12-hour light/12-hour dark cycle in a temperature and humidity-controlled environment (20–22°C, 45–55%). Mice were maintained on a chow diet (CRM(P) 801722, Special Diet Services) or fed a high fat diet (HFD) (42% from fat, TD.88137, Teklad Envigo) as detailed in the Results.

## METHOD DETAILS

### Whole exome sequencing

Whole exome sequencing data of 454,796 participants from the UK Biobank (Project number 32974) was used in this study. Data processing and quality control was performed on the Research Analysis Platform as described in Gardner et al.<sup>42</sup> Briefly, individuals were excluded for excess heterozygosity, missingness on genotyping arrays and subjects from non-European ancestry. A total of 421,065 individuals were included in the analysis. Quality controls were performed by excluding using the following criteria: SNV genotypes with 324 depth < 7 and genotype quality < 20 or InDel genotypes with a depth < 10 and genotype quality < 20. Variants were next annotated using Variant Effect Predictor v104, Revel, CADD and Loftee. Transcripts that are protein coding and listed as MANE select v0.97/VEP Canonical were prioritized for the analysis. Phenotype data was filtered for extreme values ( $\pm 5$  SD), and association testing was performed using per-gene burden test with STAAR.

### Metabolic Assessment and Meal Pattern Analysis

Mice underwent metabolic assessment measuring food intake, activity, and energy expenditure in metabolic cages (PhenoMaster, TSE, Germany). Mice were housed in open-circuit metabolic chambers measuring gas exchange (oxygen consumption and carbon dioxide production), weight of food consumed, and activity using x, y, and z plane infrared sensors. Activity heatmaps were created by multiplying the total number of beambreaks from each individual x and y infrared sensors over a 24 hr period to give spatial representation of the animal's cage activity. Meal pattern analysis was calculated using TSE software. A meal was defined as consumption of at least 20 mg and no more than 5 minutes without a bout of eating.<sup>46</sup> Meal size was calculated as the number of milligrams consumed per meal (g/meal), meal duration was the time taken to consume meals (min/meal) and eating rate was how quickly the mouse consumed meals (g/min). Meal frequency was the number of meals per day (meals/day) and the intermeal interval was defined as the average amount of time between meal events (min). Meal analysis was carried out over 3 days of chow diet and 3 days of HFD (days with cage changes were excluded from analyses) and presented as an average analysis over this period. Mice were assessed for a minimum of 120 hours where the first 48 hours were excluded for habituation. No specific method of randomization was used to assign groups, rather littermates were used where possible. Mice were assigned to experimental groups to minimize the influence of other variables such as age or sex on the outcome.

### Mouse Body Composition

Body composition including fat mass, fat free mass, bone mineral content and bone mineral density was measured by EchoMRI-500 body composition analyzer (Zinsser Analytic GmbH) or by dual-energy X-ray absorptiometry (DEXA, Lunar PIXImus). DEXA composition data was analyzed using previously reported methods.<sup>47</sup>

### Tissue Processing

Tissues were collected immediately following CO<sub>2</sub> terminal anesthesia and cervical dislocation and snap frozen in liquid nitrogen and stored at -70°C. Body length was measured *post mortem* and tissues were weighed following dissection. Liver samples for histology were dissected and immersed in 10% formalin and stored at 4°C for 48 hours before being transferred to PBS. Liver and adipose sections were processed on a Peloris Tissue Processor (Leica) and embedded in into Sakura Tissue-Tek III paraffin wax. Liver sections were cut at 40  $\mu$ m, and adipose sections were cut at 5  $\mu$ m on a microtome (Leica) and dried at 56°C overnight before being stained with H&E. For RNAscope histochemistry, mice were transcardially perfused with PBS followed by 10% formalin (Sigma-Aldrich). Brains were dissected and post-fixed in 10% formalin at 4°C for 24 hours and transferred to 30% sucrose in PBS and stored at 4°C. Brains were sectioned coronally into five equal series using a freezing sliding microtome at 25  $\mu$ m.

### Gene expression

Total RNA was extracted from frozen tissue using a standard guanidinium thiocyanate-phenol-chloroform extraction protocol or RNeasy mini kit (QIAGEN) following the manufacturer's protocol. RNA concentration was measured, and an equal quantity of RNA was reverse transcribed using M-MLV reverse transcriptase (Invitrogen). Real-Time quantitative PCR was performed on CFX384 Touch Real-Time PCR Detection System (BIORAD) using SYBR detection reagent and primers designed for each gene of interest. Results of each gene of interest were normalized to the geometric mean of two stable reference genes and no template controls and no reverse transcriptase controls were run for each gene. Primers used are as follows; Collagen 1

FW-5'-CCAAAGGTGCTGATGGTTCT-3', RV-5'-ACCAGCTTACCCTTGTCAC-3'; Collagen 2: FW-5'-CCTCAAGGCAAAGTTGGT CCT-3', RV-5'-GGCTCCAGGAATACCATCAGT-3'; Fabp4: FW-5'- CAAACTGGGCGTGGAATTCG-3', RV-5'-ACCAGCTTGTCAACC ATCTCG-3'; Gpr75 (5-bp Deletion): FW-5'-TAAACATGCCTCCCCTGCACG-3', RV-5'-GATGGCAAGCAGAAAAGTGC-3'; Gpr75: FW-5'- TCTTCTTTGGCACATGCTCG-3', RV-5'- CACTGGACGTGAAAAGACGA-3'; Hprt: FW-5'- GTTAAGCAGTACAGCCCCA AA-3', RV-5'- AGGGCATATCCAACAACAACTT-3'; Nono: FW-5'- GCCAGAATGAAGGCTTGACTAT-3', RV-5'- TATCAGGGGGA AGATTGCCCA-3'; Pgc1a: FW-5'- AGCCTCTTTGCCAGATCTT-3', RV-5'- GGCAATCCGTCTTCATCCAC-3'; Pparg: FW-5'-CAG ACCTCAGGCAGATCGTC-3', RV-5'-GAAGGAACACGTTGTCAGCG-3'; TIMP1: FW-5'-GCAACTCGGACCCTGGTCATAA-3', RV- 5'-CGCCCCGTGATGAGAACT-3'; Ywhaz: FW-5'- GAAAAGTTCTTGATCCCCCAATGC-3', RV-5'- TGTGACTGGTCCACAATTCCT T-3'. For the detection of Ucp1 a TaqMan qPCR probe was used: Mm01244861 m1 (ThermoFisher).

### Western Blot

Liver samples were homogenized in lysis buffer containing protease inhibitors (Thermo). The concentration of the protein lysates was determined by BCA assay (Thermo). Proteins were separated by standard SDS-PAGE and transferred to PVDF membrane. Protein expression was detected using the following antibodies: aSMA (Abcam, ab21027), B-Tubulin (Cell Signalling, D3U1W), anti-mouse IgG HRP-linked secondary (Cell Signalling, 7076S), and rabbit anti-goat IgG (Abcam, ab6697). Membranes were visualised using ECL detection reagent (Thermo) and quantified using ImageJ software (NIH).

### Histology Analysis

Histology and RNAscope in situ hybridization (ISH) sections were imaged using Axioskop 2 Mot Plus microscope (Zeiss, Germany) and analyzed using ImageJ (NIH). Liver histology was analyzed from four images per animal using the trainable weka segmentation tool<sup>44</sup> to separate the image into lipid or background using 25 reference segments. A probability map was generated and transformed to a binary image. The lipid content was calculated from each image.

### Triglyceride assay

Liver triglyceride content was measured from frozen tissue lysates. Frozen liver samples were weighed prior to homogenization in PBS. Lysates were centrifuged at 12,000xg for 10 minutes at 4°C before the supernatant was extracted. Triglyceride levels were determined against a standard curve using Triglyceride Liquid Assay (Sentinel Diagnostics). Each sample was then normalized to individual tissue weights.

### RNAscope ISH

A series of a full mouse brain was mounted on SuperFrost Plus slides and air-dried at room temperature. Slides were treated and detected using DAB staining according to the manufacturers protocol (RNAscope 2.5 HD Assay Detection, Advanced Cell Diagnostics) using *Gpr75* probe (Cat. 318281, Advanced Cell Diagnostics). Negative control probe targeting *DapB* gene was also run for each RNAscope ISH experiment.

### Single cell RNA sequencing

The clustered mouse hypothalamus single nucleus RNA sequencing data (generation described in 8) and RNA sequencing data is available from (<https://doi.org/10.17863/CAM.87955>). Hypomap dataset from Steunernagel et al.<sup>10</sup> was used for analysis of *Gpr75* transcript expression in the mouse hypothalamus. Analysis was performed using the Seurat package version 4.0.3/R 4.1.<sup>43</sup> Nuclei expressing at least one  $\geq 1$  UMI count for *Gpr75* gene were identified as *Gpr75*<sup>+IVE</sup> cells. The feature plots were generated using the Seurat package and ggplot2.

## QUANTIFICATION AND STATISTICAL ANALYSIS

### Statistical analysis

Raw data were inputted into or transferred to Excel (Microsoft) files. Plots and statistical analyses were generated in GraphPad Prism 9.4 (GraphPad Software). Data has been analyzed using unpaired two-tailed Student's t test, one-way analysis of variance (ANOVA), or two-way or mixed model analysis of variance (ANOVA) as required and detailed in the results. Where appropriate, data are presented as individual data points, and summary data are presented as mean  $\pm$  SEM. Details of statistical tests results and number of animals can be found in the figure legends. Statistical significance was defined as \*p < 0.05, \*\*p < 0.01, \*\*\*p < 0.001 and \*\*\*\*p < 0.0001.